In Situ Scanning Probe Microscopy Studies of Tetanus Toxin-Membrane Interactions

Andrea L. Slade,* Joseph S. Schoeniger,† Darryl Y. Sasaki,‡ and Christopher M. Yip*
*Department of Biochemistry, Department of Chemical Engineering and Applied Chemistry, Institute of Biomaterials and Biomedical Engineering, University of Toronto, Toronto, Ontario, Canada; †Sandia National Laboratories, Biosystems Research, Livermore, California; and ‡Sandia National Laboratories, Biomolecular Interfaces & Systems, Albuquerque, New Mexico

ABSTRACT Despite the considerable information available with regards to the structure of the clostridial neurotoxins, and their inherent threat as biological warfare agents, the mechanisms underpinning their interactions with and translocation through the cell membrane remain poorly understood. We report herein the results of an in situ scanning probe microscopy study of the interaction of tetanus toxin C-fragment (Tet C) with supported planar lipid bilayers containing the ganglioside receptor G_{T1b}. Our results show that Tet C preferentially binds to the surface of fluid phase domains within biphasic membranes containing G_{T1b} and that with an extended incubation period these interactions lead to dramatic changes in the morphology of the lipid bilayer, including the formation of 40–80 nm diameter circular cavities. Combined atomic force microscopy/total internal reflection fluorescence microscopy experiments confirmed the presence of Tet C in the membrane after extended incubation. These morphological changes were found to be dependent upon the presence of G_{T1b} and the solution pH.

INTRODUCTION

Recent concern regarding biological toxins, such as tetanus (TeNT) and botulinum neurotoxin (BoNT), has arisen from their potential use as biological weapons (1,2). Characterizing the dynamics of their interactions at the membrane interface may therefore provide insights into the development of new treatments, detection strategies, and prophylactic agents. The *Clostridial* neurotoxins are the most potent toxins known, with TeNT and BoNT responsible for the clinical symptoms of tetanus and botulism, respectively. These toxins target neuronal cells by binding to the trisialoganglioside G_{T1b} in the presynaptic cell membrane of neuromuscular junctions (3,4), and are internalized into the cells where they ultimately inhibit neurotransmitter release (5). However, while BoNTs act primarily in the peripheral nervous system blocking acetylcholine release, TeNT undergoes axonal retrograde transport to the central nervous system where it targets inhibitory motor neurons (6,7). TeNT is synthesized by the bacterium *Clostridium tetani* as a single ~150 kDa polypeptide chain that must undergo posttranslational proteolytic cleavage to produce the biologically active, disulfide linked two-chain molecule that is composed of an ~50-kDa light chain (LC) and an ~100-kDa heavy chain (HC) (Fig. 1 *a*) (8). The binding of tetanus toxin to G_{T1b} in neuronal cell membranes is mediated by the ~50-kDa C-terminal region (H_C) of the heavy chain, known as the C fragment (Tet C) (Fig. 1 *b*). The ~50-kDa N-terminal region (H_N) facilitates the translocation of the LC, a zinc endopeptidase, into the cell cytosol. Once in the cytosol, the LC specifically cleaves the synaptic SNARE (soluble *N*-ethylmaleimide sensitive-factor attachment protein receptor) protein synaptobrevin, thereby preventing the fusion of neurotransmitter secretory vesicles to the nerve terminal membrane, and thus blocking the release of inhibitory neurotransmitters (9).

In general, invasion of a host cell by the bacterial A_nB_m-toxins, which includes diphtheria toxin, cholera toxin, botulinum A & B toxins, and tetanus toxin involves four general stages: 1), cell surface binding; 2), internalization; 3), membrane translocation into the cytosol of the host; and 4), modification of a cytosolic target. With respect to this process of cell intoxication, the mechanisms of toxin internalization and membrane translocation are the least understood. While it is generally accepted that toxin molecules are internalized via endocytosis of the regions of the cell membrane to which they are bound, the mechanism of membrane translocation, however, appears to differ among the classes of toxin molecules. In the case of the TeNT, it is believed that following endocytosis, lowering of the pH inside the endosome triggers a conformational change that increases the hydrophobicity of the toxin molecule (10,11). This conformational change facilitates insertion of TeNT into the endosomal membrane with subsequent translocation of the light chain into the cytosol, where it exerts its catalytic activity. Indeed, it has been reported that A_nB_m-toxins having A_1B_1-stoichiometry, including the full-length tetanus toxin, form ion channels in planar lipid bilayers at acidic pH (12–18).

To fully understand how toxins exert their action, it has been proposed that ''trapping'' the toxin molecules at different points along the invasion pathway from the cell surface to the cytosol, would allow for reconstruction of the entire mechanism (19). Although this approach has been applied successfully to characterize colicin Ia activity, it is extremely arduous and time intensive (20). Recently, in situ studies

Submitted December 27, 2005, and accepted for publication August 22, 2006.

Address reprint requests to Christopher M. Yip, IBBME, Rosebrugh Bldg., University of Toronto, 4 Taddle Creek Rd., Toronto, Ontario, Canada, M5S 3G9. Tel: 416-978-7853; Fax: 416-978-4317; E-mail: christopher.yip@utoronto.ca.

0006-3495/06/12/4565/10 $2.00

doi: 10.1529/biophysj.105.080457

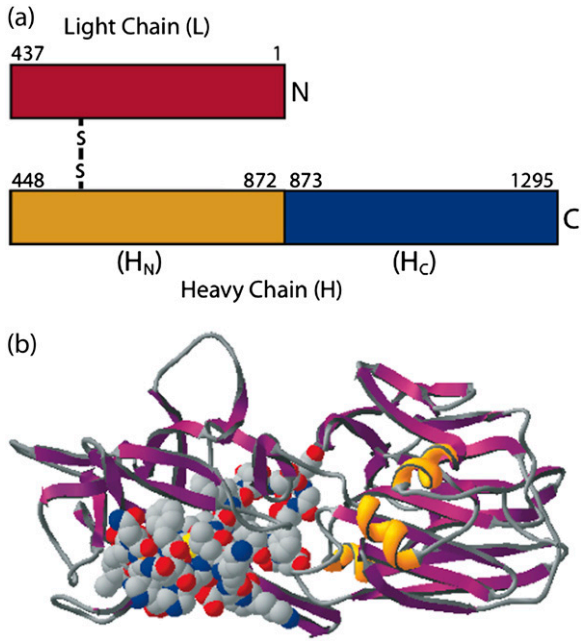

FIGURE 1 The structures of the clostridial neurotoxins: tetanus neurotoxin (TeNT) and botulinum neurotoxin (BoNT). All models are shown as ribbon structures. (*a*) The active form of the clostridal neurotoxins is a two-chain molecule composed of a disulfide-linked light chain (*C*) and heavy chain (*H*). The light chain is the catalytic domain, while the C-terminal domain (H_C) and the N-terminal domain (H_N) of the heavy chain mediate binding to neuronal cell membranes and translocation of the light chain, respectively. (*b*) The C-terminal domain of tetanus toxin, otherwise known as the Tet C-fragment. The last 34 residues of Tet C are involved in ganglioside recognition (residues shown as CPK space-fill). The image is based on PDB model 1FV2 and was prepared using the Swiss PDB Viewer molecular graphics software package (GlaxoSmithKline).

using scanning probe microscopy (SPM), and more specifically, atomic force microscopy (AFM), have provided new insights into the association and assembly of various peptides and proteins, such as filipin (21), amphotericin B (22), and melittin (23), on membrane surfaces, including their role in inducing membrane reorganization and disruption. We have used this technique to study the insertion and subsequent assembly of the amyloid-β 42 (Aβ42) peptide (24), α-synuclein (25), hemagglutinin (26), Bax protein (27), and NAP22 (28) at membrane interfaces.

For such studies, supported planar lipid bilayers (SPBs) are often used as membrane-mimetic surfaces. Typically prepared in situ by free vesicle fusion onto a freshly cleaved mica surface, SPBs retain many of the properties of free-standing membranes, including lateral fluidity (29–31). Indeed, direct fusion of receptor-containing lipid vesicles onto mica is a particularly facile and attractive route of preparing model membranes for AFM studies of ligand-receptor interactions. We have used this approach in our earlier investigation of the full-length transmembrane insulin receptor (IR) (32).

We report herein an in situ AFM study on the interactions of the tetanus toxin binding domain (Tet C) with biphasic supported planar lipid bilayers containing the ganglioside membrane receptor G_{T1b}. Our results revealed preferential association of Tet C with the surface of the fluid phase regions of the lipid bilayers, and that the affinity was dependent upon the bilayer concentration of G_{T1b} and solution pH. Following an incubation period, the protein-bound regions of the membrane became thicker and circular depressions of 40–80 nm diameters appeared through the action of Tet C upon the membrane. The presence of Tet C in these regions of the bilayer was confirmed using combined atomic force microscopy/total internal reflection fluorescence microscopy (AFM/TIRFM) (33). From these studies, detailed insights into the binding and activity of Tet C and subsequent restructuring of the lipid bilayer were attained at nanoscale resolution.

MATERIALS AND METHODS

Materials

1,2-Dipalmitoleoyl-*sn*-glycero-3-phosphocholine (DPOPC; C16:1) was purchased from Avanti Polar Lipids (Alabaster, AL). Trisialoganglioside G_{T1b}, tetanus toxin C fragment (Tet C), fluorescein isothiocyanate (FITC) labeled tetanus toxin C fragment (FITC-Tet C; 495 nm/525 nm), and DL-α-dipalmitoyl-phosphatidylcholine (DPPC; C16:0) were purchased from Sigma-Aldrich (Oakville, ON).

Liposome preparation

Appropriate molar quantities of lipid ((1:1) DPOPC/DPPC) and, when required, the desired amount of G_{T1b} (10 mol % or 1 mol %) were dissolved in chloroform. During preparation, fluorescent liposomes were protected from light to minimize photobleaching. The solvent was removed by evaporation under vacuum (~50°C) and the dried lipid films were rehydrated by the addition of 5 mM (*N*-2-hydroxyethylpiperazine-*N*-2-ethanesulfonic acid)-(2-[*N*-morpholino] ethanesulfonic acid)-citric acid (HEPES-MES-citric acid) buffer (150 mM NaCl, pH 7.4) to give a final lipid concentration of 2 mM. Unilamellar vesicles were then formed by sonication in a heated water bath (~50°C) (Branson 200, Branson Ultrasonics, Danbury, CT) until the solution became clear or only slightly hazy. The resulting liposomes were found to be ~145 nm in diameter by dynamic laser light scattering (Brookhaven Instruments BI-200SM equipped with a BI-9000 AT digital correlator and photon counter; Holtsville, NY). The fluorescent liposome solutions were stored in the dark. All liposome solutions were stored at 4°C.

AFM imaging

Solution tapping mode AFM (TMAFM) images were acquired on a Digital Instruments Nanoscope IIIa Multimode SPM (Santa Barbara, CA) equipped with an ''E'' scanner (13.6 × 13.6 μm maximum lateral scan area) using 120-μm-long oxide-sharpened silicon nitride V-shaped model DNP-S cantilevers installed in a combination contact/tapping mode liquid flow-cell sealed against a freshly cleaved mica substrate. The typical tip oscillating frequency was 7–9 kHz and was chosen to optimize image quality and adjusted for the individual response characteristics of each cantilever. We note that the nominal radius of curvature of the DNP-S tips used in these studies was ~15 nm, and that for each experiment, a fresh tip was selected and exposed to ultraviolet irradiation to remove any adventitious organic contaminants prior to imaging. All AFM images were collected as 512 × 512 pixel data sets, at scan rates ranging from 1 to 2 Hz, at a scan angle of 0° to the fast scan axis, and at ambient temperature. For the Tet C studies on mica, ~150 μL of a 5 μg/mL Tet C solution (10 mM PBS, 150 mM NaCl,

pH 7.4) was applied to the mica surface and the sample sealed in the AFM fluid cell. The fluid cell was flushed through with protein-free buffer after a 30-min incubation period. The sample remained fully hydrated during the incubation period. Supported planar lipid bilayers were formed in situ by injecting ~200 μL of the G_{T1b}/DPOPC/DPPC or DPOPC/DPPC liposome solution directly into the fluid cell and allowing it to adsorb to the mica surface for ~10 min. The fluid cell was then flushed with 10 mM $CaCl_2$ solution to facilitate liposome fusion. Once the bilayers were formed, calcium ions and excess lipid were removed by flushing the fluid cell with 10 mM ethylenediaminetetraacetic acid (EDTA) solution. Before the introduction of Tet C, reference images of the lipid bilayers were acquired in 5 mM HEPES-MES-citric acid buffer (pH 7.4). For the Tet C-membrane interaction studies, ~300 μL of a 10 μg/mL HEPES-MES-citric acid solution (pH 7.4) of Tet C was injected directly into the fluid cell and imaging initiated after ~1 h. In the case of experiments carried out at pH 4.0, the Tet C-free bilayers were formed at pH 7.4 and the imaging fluid exchanged with 5 mM HEPES-MES-citric acid buffer (pH 4.0) before the addition of Tet C. For these studies, the 10 μg/mL Tet C solution was also made up in 5 mM HEPES-MES-citric acid buffer (pH 4.0). All AFM imaging experiments were repeated five times.

Combined AFM/TIRFM imaging

Solution tapping mode atomic force microscopy/total internal reflection fluorescence microscopy (TMAFM/TIRFM) images were acquired on a Digital Instruments Nanoscope IIIa Bioscope SPM equipped with an extended z-range ''J'' scanner (116 × 116 μm maximum lateral scan area) and mounted on an Olympus Fluoview 500 confocal microscope equipped with an Olympus TIRFM accessory (10 mW Ar-ion (488 nm) laser (Melles Griot, CA); Olympus 60× 1.45 NA TIRFM objective). All TIRFM images were acquired simultaneously using a cooled charge-coupled device camera (CoolSnap HQ, Roper Scientific, Tucson, AZ) and the Image Pro Plus software package (Media Cybernetics, Silver Springs, MD). Oxide-sharpened silicon nitride V-shaped cantilevers (120 μm) were installed in a combination contact/tapping mode liquid cell and supported planar lipid bilayers were formed in situ by the introduction of ~200 μL of a 10 mol % G_{T1b}/DPOPC/DPPC liposome solution directly onto a freshly cleaved mica surface that was sealed within a custom-built thermostated flow cell. The flow cell was fitted with a motorized syringe pump (Harvard Apparatus, Saint-Laurent, Quebec, Canada) to facilitate exchange of imaging solutions. The liposomes were allowed to adsorb to a mica surface for ~10 min and then ~200 μL of a 10 mM $CaCl_2$ solution was then added to aid liposome fusion. Once the bilayers had formed, the flow cell was flushed several times sequentially with 10 mM EDTA solution and 5 mM HEPES-MES-citric acid buffer (pH 7.4) to remove calcium ions and any excess lipid. All AFM/TIRFM imaging was conducted in complete darkness at ambient temperature in 5 mM HEPES-MES-citric acid buffer (pH 7.4). For the fluorescently labeled Tet C studies, ~200 μL of a ~25 μg/mL HEPES-MES-citric acid buffer solution (pH 7.4) of FITC-Tet C was added to the fluid cell. The FITC-Tet C solution contained ~5 μg of bound FITC per milligram of Tet C, as stated by the manufacturer. Imaging was initiated after ~1 h incubation. Five replicate AFM/TIRFM experiments were performed.

AFM image analysis

Image analyses were conducted using the Digital Instruments Nanoscope software (version 4.42r9). Height images were low-pass filtered and plane-fit in the x-scan direction. Quantitative height measurements were determined by section analysis.

Molecular modeling

Images were prepared using Swiss PDBViewer, Version 3.7b2 (http://www.expasy.org/spdbv/). The Tet C and BoNT B molecular coordinates were obtained from the Protein Data Bank (PDB) using the identification codes 1FV2 and 1SOF, respectively.

RESULTS AND DISCUSSION

AFM imaging of Tet C adsorbed to mica

Although the three-dimensional crystal structure of the tetanus toxin C-fragment (Tet C) complexed with a trisialoganglioside G_{T1b} analog receptor has been solved (34), there have been no reported structural studies of Tet C bound to its native receptor in a membrane or membrane-mimetic environment. To establish a structural baseline, we first characterized Tet C as an adsorbed species on a mica surface. After ~30 min incubation in the presence of a ~5 μg/mL solution of Tet C, tapping mode AFM (TMAFM) imaging of the mica surface revealed small, randomly distributed particles with a height of ~3.5 nm and widths ranging from ~15 to ~40 nm (Fig. 2 *a*). Electrostatic potential maps of the Tet C surface reveal a large area of negative charge (red area) opposite to the ganglioside-binding site, which is an area of concentrated positive charge (blue area) (Fig. 2 *b*). As mica is negatively charged at neutral pH, it is likely that Tet C would adsorb in an orientation such that the area of positive charge, or the ganglioside-binding site, would interact with the mica surface. This orientation would presumably be similar to that with which Tet C interacts with its ganglioside receptor and is consistent with the structures observed on mica by TMAFM. We note that although AFM tip-sample convolution does contribute to significant overestimation of the lateral dimensions of adsorbed molecules (35), image deconvolution of these structures using a nominal tip size of ~15 nm was consistent with the adsorption of Tet C, as single molecules, to the mica surface.

AFM imaging of Tet C interactions with lipid bilayers

For our studies of Tet C-membrane interactions, SPBs were formed by in situ fusion of an equimolar (1:1) DPOPC/DPPC liposome solution containing 10 mol % G_{T1b}. We have previously shown that the fusion of ganglioside-free DPOPC/DPPC liposomes to mica results in the formation of a phase-separated lipid bilayer consisting of gel phase DPPC microdomains surrounded by a fluid phase DPOPC lipid matrix (33). In this study, solution tapping mode AFM (TMAFM) imaging of the 10 mol % G_{T1b}-containing DPOPC/DPPC lipid bilayers revealed molecularly smooth bilayers that were composed of two types of membrane structures, with tall domains extending ~1.5 nm above a shorter continuous lipid phase (Fig. 3). The lipid bilayers themselves were fairly continuous across the AFM imaging window, with only the occasional defect exposing the underlying mica surface. Cross section analysis performed at the edges of these defect areas revealed the shorter continuous phase to

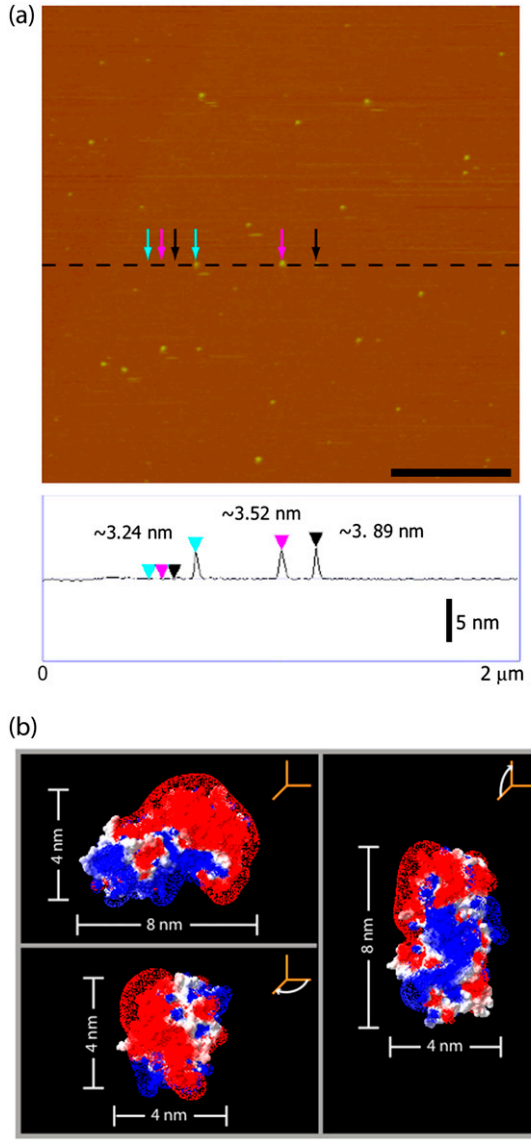

FIGURE 2 (*a*) In situ TMAFM topography (height) image of Tet C adsorbed on a mica surface. Cross section analysis found the Tet C molecules to have a height of ~3.5 nm and widths of 9–32 nm. The AFM image is height-encoded by color where lighter colors correspond to taller features. Height scale, 20 nm; scale bar, 500 nm. (*b*) Electrostatic potential surface maps of the Tet C crystal structure oriented at Tet C is believed to interact with the mica surface. Based on these structures, Tet C is believed to adsorb onto the mica surface as single molecules and in an orientation similar to that with which it binds to the G_{T1b} receptor. (*red*, areas of negative charge; *blue*, areas of positive charge.) Images are based on PDB model 1FV2 and prepared using the Swiss PDB Viewer molecular graphic software package (GlaxoSmithKline).

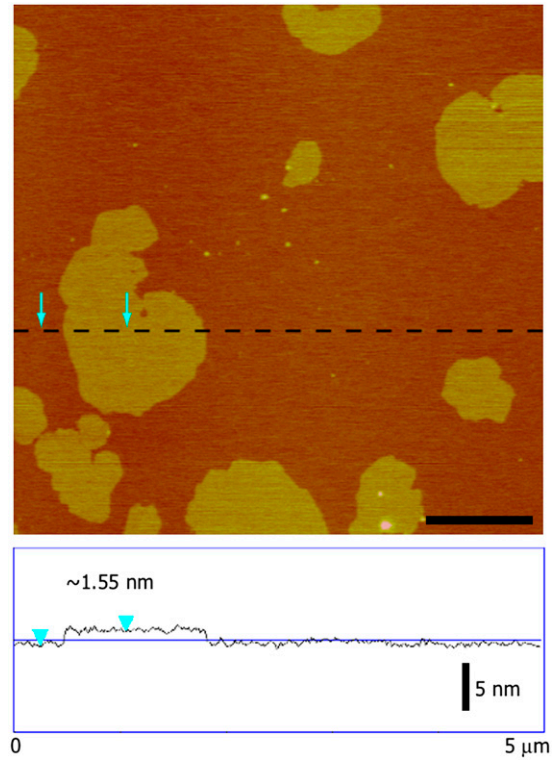

FIGURE 3 In situ TMAFM topography (height) imaging of 10 mol % G_{T1b}/DPOPC/DPPC supported planar lipid bilayers revealed a biphasic membrane structure with DPPC-rich domains extending ~1.5 nm in height above the surrounding by a DPOPC-rich lipid matrix. No structures were observed in the bilayer that could be attributed to the presence of G_{T1b}. The AFM image is height-encoded by color where lighter colors correspond to taller features. Height scale, 20 nm; scale bar, 1 μm.

be ~5.5 nm tall (for example, see Fig. 4 *a*). These results are consistent with previous AFM studies of binary lipid systems where the ~1.5 nm height difference has been attributed to a decrease in the tilt angle of the acyl chains of the gel phase lipids due to tighter packing of the hydrophobic tails (36–40). As such, these data are in agreement with the taller domains being rich in DPPC and the shorter regions of the membrane being rich in DPOPC. We cannot discount the possibility of transient bilayer defects that exist on timescales shorter than that which can be readily resolved by the AFM.

AFM images of DPOPC/DPPC (1:1) bilayers containing 10 mol % G_{T1b} showed no differences from those acquired on control bilayers lacking the ganglioside (33). Even at high resolution, no features were found that could be attributed to aggregates of G_{T1b}. It is known that gangliosides, as well as other glycosphingolipids, and cholesterol are involved in the formation of ''lipid raft'' membrane domains. These structures are thought to play a leading role in regulating membrane function and have been implicated in mediating molecular recognition and intracellular signal transduction (41–44). In the past, evidence of such domains has often been obtained by direct imaging of complexes between the ganglioside receptors and their corresponding ligand. In the case of monosialoganglioside G_{M1}, this has been accomplished through the introduction of soluble cholera toxin B-subunits (CTX-B). For instance, Mou et al. performed AFM studies on the CTX-B-G_{M1} complex to infer that G_{M1} was homogeneously distributed throughout gel phase dipalmitoylphosphatidylcholine

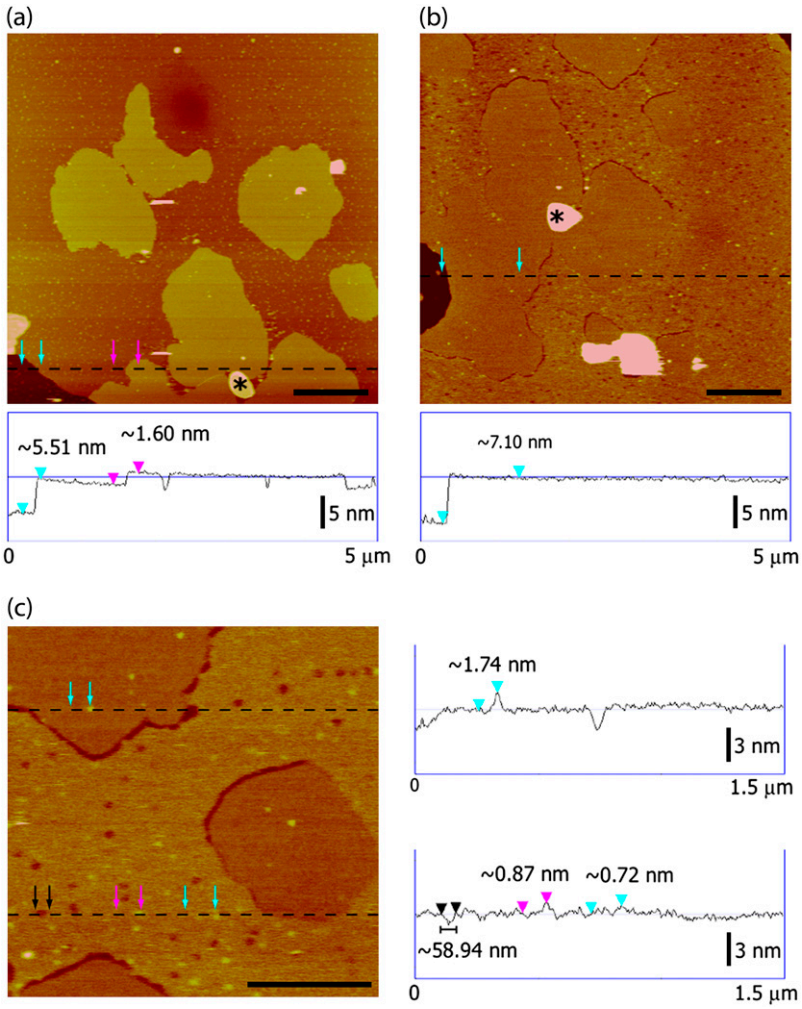

FIGURE 4 In situ TMAFM topography (height) imaging of the interactions between Tet C and 10 mol % G_{T1b}/DPOPC/DPPC supported planar lipid bilayers. (*a*) After ~2 h exposure, Tet C appeared to be preferentially associated with regions of DPOPC and was distributed relatively homogeneously throughout the fluid phase domains. (*b* and *c*) After ~12 h exposure, TMAFM topography (height) imaging of the same region of the lipid bilayer (as indicated by the *asterisk*) revealed a dramatic change in the bilayer morphology. The DPOPC-rich regions appeared to have a granular texture and were populated by a number of circular defects having widths of 40–80 nm. The height of the DPOPC regions had also increased to that of the DPPC domains, with the DPPC domains now appearing to be encircled by line defects. The DPPC domains themselves appeared relatively unchanged. Cross section analysis revealed that the Tet C molecules associated with DPPC domains extend ~2 nm above the surface of the gel phase domains. Tet C molecules that were associated with fluid phase DPOPC, however, extended <1 nm above the surface of the bilayer, suggesting partial insertion of Tet C within the regions of DPOPC. The amount of Tet C associated with the bilayer at ~12 h incubation appeared to be much lower than at ~2 h incubation. The AFM images are height-encoded by color where lighter colors correspond to taller features. Height scale, panels *a* and *b* = 20 nm, panel *c* = 12 nm; scale bar, panels *a* and *b* = 1 μm; panel *c* = 500 nm.

(DPPC) bilayers (45). In yet other AFM studies, Yuan and Johnston used CTX-B as a reporter molecule to confirm clustering of G_{M1} receptors in DPPC monolayers and bilayers as well as in fluid phase egg-PC lipid bilayers (46,47). To date, there has been very little work done to characterize the distribution of G_{T1b} in bilayers although we note that electron microscopy has been used to visualize G_{T1b} in phosphatidylcholine bilayers using lectin molecules as topographical markers (48).

Although the presence of G_{T1b} was not confirmed by AFM imaging, its presence was verified through binding studies with Tet C. In the absence of G_{T1b}, Tet C did not exhibit any affinity for the DPOPC/DPPC bilayers with no changes observed in the bilayer surface topology or structural morphology after ~12 h exposure to a 10 μg/mL solution of Tet C (data not shown). Under the same conditions, in situ TMAFM revealed a structural topology of DPOPC/DPPC bilayers containing 10% G_{T1b} that suggests adsorption of Tet C with selective affinity for the DPOPC-rich areas after ~2 h incubation (Fig. 4 *a*). These regions of the bilayer were populated by numerous protrusions having dimensions that are consistent with bound Tet C molecules. The bound proteins were homogeneously distributed throughout the fluid phase DPOPC extending ~2 nm above the bilayer surface. The relatively featureless surface of the areas rich in DPPC suggests little adsorption of Tet C to these gel phase areas, although further confirmation was attained via fluorescence imaging (vide infra).

TMAFM imaging of the same area of the bilayer after ~12 h of exposure revealed a dramatic change in the overall bilayer morphology (Fig. 4 *b*). While the DPPC-rich domains remained relatively unchanged, the previously smooth DPOPC-rich areas now had a granular texture and were populated by numerous small, circular cavities with diameters in the range of 40–80 nm (Fig. 4 *c*). These changes in the overall structure of the membrane are clearly evident in the three-dimensional image of the bilayer surface shown in Fig. 5. Cross section analysis also revealed that after ~12 h the DPOPC-rich lipid phase now exhibited a thickness similar to that of the DPPC domains (~7 nm). In addition to the cavity formation and the thickening of the DPOPC lipid phase, the Tet C molecules bound to the surface of the

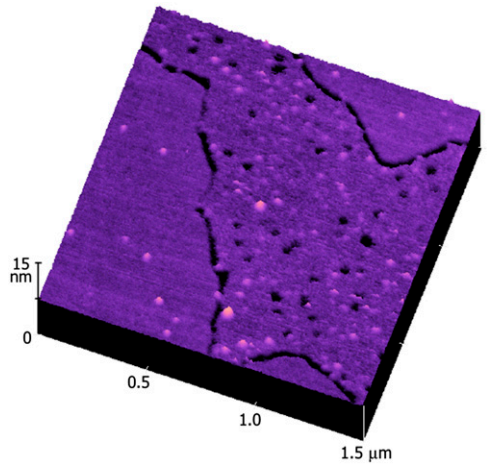

FIGURE 5 Three-dimensional 1.5 × 1.5 μm TMAFM topography (height) image of a 10 mol % G_{T1b}/DPOPC/DPPC lipid bilayer after ~12 h incubation in the presence of the Tet C fragment. The AFM image is height-encoded by color where lighter colors correspond to taller features. Height scale, 15 nm.

DPOPC-rich regions were also found to have decreased in height (<1 nm in height). Upon closer examination, the small number of Tet C aggregates occasionally found on the surface of the DPPC domains exhibited no change in height nor induced any structure changes on that portion of the membrane after ~12 h of incubation (Fig. 4 *c*). In control studies performed with supported lipid bilayers of the same composition (10 mol % G_{T1b}/DPOPC/DPPC), no change or obvious disruption of the bilayers was observed after ~12 h of TMAFM imaging in the absence of Tet C (data not shown).

These observations suggest that over the 12-h incubation period the Tet C molecules have either become partially embedded in the fluid DPOPC regions or the Tet C molecules have dissociated from the bilayer surface. To resolve this question, we performed a correlated TMAFM/TIRFM imaging study on 10 mol % G_{T1b}/DPOPC/DPPC lipid bilayers that had been exposed to a ~25 μg/mL solution of FITC-labeled Tet C fragment (FITC-Tet C). After in situ fusion of the G_{T1b}/DPOPC/DPPC lipid vesicles on the mica surface, TMAFM imaging revealed well-formed phase-separated lipid bilayers with a morphology similar to those previously described. There was no observable autofluorescence from these lipid bilayers when TIRFM imaging was performed (data not shown). After ~12 h incubation of the bilayers with FITC-Tet C, in situ TMAFM imaging revealed that the DPOPC regions were again granular in texture and populated by numerous circular cavities, whereas the DPPC domains remained relatively unchanged (Fig. 6 *a*). The corresponding TIRFM images, acquired simultaneously, revealed a bright fluorescence emission from the DPOPC regions, which is consistent with preferential association of the FITC-Tet C with the fluid lipid phase (Fig. 6 *b*). We note that TIRFM data acquired during intermediate time points was consistent with the association of the FITC-Tet C with the bilayer.

Although correlated TIRFM imaging confirms the presence of Tet C within the DPOPC regions, it is important to note that we were unable to resolve the Tet C molecules on

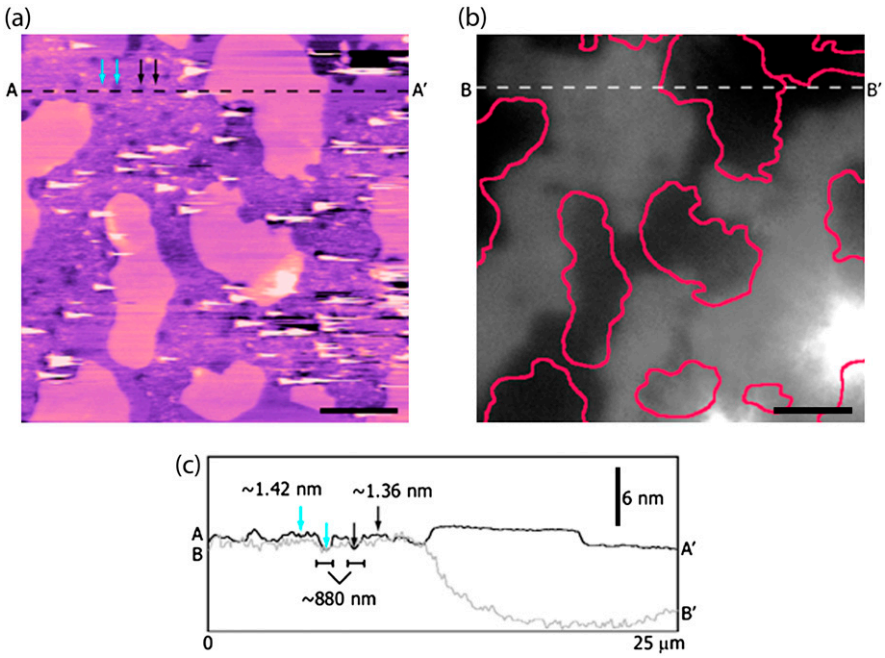

FIGURE 6 Combined AFM/TIRFM imaging of the interactions between FITC-labeled Tet C and 10 mol % G_{T1b}/DPOPC/DPPC lipid bilayers. (*a*) After ~12 h incubation in the presence of FITC-Tet C, in situ TMAFM topography (height) imaging revealed the fluid phase DPOPC-rich regions to have a granular texture and were populated by a number of circular defects. The AFM image is height-encoded by color where lighter colors correspond to taller features. Height scale, 18 nm; scale bar, 5 μm. (*b*) TIRFM imaging of the same region of the bilayer revealed that the bright fluorescent regions correlated with the DPOPC regions in the TMAFM image, whereas dark nonfluorescent regions correlated with the DPPC domains. For better visualization, the DPPC domains in the TMAFM image are outlined in pink in the TIRFM image. The two bright fluorescent areas in the bottom right-hand corner of the TIRFM image correspond to the position of two 200-nm diameter Fluosphere microspheres (Molecular Probes) that were used to focus the TIRFM objective on the mica surface before introduction of the lipid vesicles into the fluid cell. Scale bar, 5 μm. (*c*) Cross section profiles of the correlated regions in the TMAFM height image (A–A′) and the TIRFM image (B–B′). The circular defects observed in the DPOPC regions were found to have widths of 600–900 nm and a depth of ~1.5 nm. The larger size of these defects may be due to the higher concentration of FITC-Tet C used in these studies.

these domains using in situ TMAFM. The two bright fluorescent areas in the bottom right-hand corner of the TIRFM image correspond to the position of two 200-nm diameter Fluosphere microspheres (Molecular Probes, Eugene, OR) that were used to focus the TIRFM objective on the mica surface before introduction of the lipid vesicles into the fluid cell. We note that the TIRFM and AFM data sets are not perfectly correlated. This is likely a consequence of a nonuniform distribution of the GT_1B receptor in the fluid phase of the supported bilayer and hence, the distribution of the FITC-Tet C molecules bound to G_{T1b} (49,50). We also cannot discount the possibility that the dynamics of the lipid bilayer may be better resolved on TIRFM timescales rather than on AFM imaging timescales (33).

The results of our correlated TMAFM/TIRFM study suggest that after continuous incubation of Tet C with the 10 mol % G_{T1b}/DPOPC/DPPC lipid bilayers, the surface-bound Tet C undergo partial insertion into the G_{T1b}-containing DPOPC fluid phase regions of the bilayer, thus explaining both the decrease in height and the apparent decrease in the surface coverage of Tet C in these areas. The absence of Tet C within the gel-phase DPPC domains may be due to the tighter packing of the DPPC molecules, which prevents protein insertion, or due to an absence of G_{T1b} in the DPPC domains. Similar studies using 10 mol % G_{T1b}/DPPC lipid bilayers also revealed no G_{T1b}-induced clustering or domain formation nor any specific association of Tet C molecules with these surfaces after extended incubation periods (data not shown). Although the preferential association with the DPOPC-rich regions observed for Tet C may reflect favorable partitioning of the G_{T1b} receptors into the fluid phase regions of the lipid bilayers, it is also possible that it may simply reflect a greater degree of mobility of the receptors within the fluid DPOPC matrix, and hence greater ease in adopting the correct binding conformation. Although it would be ideal to use combined TMAFM/TIRFM to address the issue as to the presence/absence of G_{T1b} within the DPPC lipid domains, it is becoming increasingly apparent that the behavior of a fluorescently labeled lipid is strongly influenced by the presence of the fluorophore (51–53). The addition of a bulky fluorophore to the acyl chain of a ganglioside or phosphocholine molecule prevents tight packing of the lipid tails, and thus often results in the formation of, or partitioning of the fluorescent probe into, a more disordered phase in the lipid bilayer. Similar behavior has also been observed for headgroup labeled lipids (54,55). As such, under the conditions of our studies, we are unable to quantitatively determine the partitioning of G_{T1b} in either lipid phase.

In situ TMAFM studies were also conducted to examine the effect of varying the G_{T1b} concentration and the pH of the surrounding imaging fluid on Tet C-membrane interactions. In the case of DPOPC/DPPC bilayers containing 1 mol % G_{T1b}, the Tet C molecules were also found to be preferentially associated with the DPOPC-rich areas after an initial ~2-h incubation period. In contrast to our studies of the 10 mol % G_{T1b}/DPOPC/DPPC bilayers after exposure to Tet C (vide infra), after ~12 h of incubation with Tet C, we saw no evidence of persistent defects in either lipid phase of the 1 mol % G_{T1b}/DPOPC/DPPC bilayers (Fig. 7). Cross section analysis revealed the Tet C molecules associated with the DPOPC-rich regions after ~12 h to have a height of ~2 nm relative to the surface of the bilayer. The occasional Tet C molecule was also observed on the surface of the DPPC domains with a height of ~2 nm.

Under acidic conditions (pH 4.0), Tet C did not appear to associate with the 10 mol % G_{T1b}/DPOPC/DPPC lipid bilayers (data not shown). This may be due to a conformational change in Tet C, a structural change in the G_{T1b} headgroup, or a change in the electrostatic interaction between the ganglioside and the protein that prevented successful binding of Tet C to G_{T1b} (10,11). These data are consistent with those of Winter et al. who reported that the full-length TeNT preferentially bound to negatively charged lipids in vesicles (56). Based on the results of their studies into the interactions of TeNT with vesicles containing different types of lipid molecules, Winter et al. believed that successful binding of the

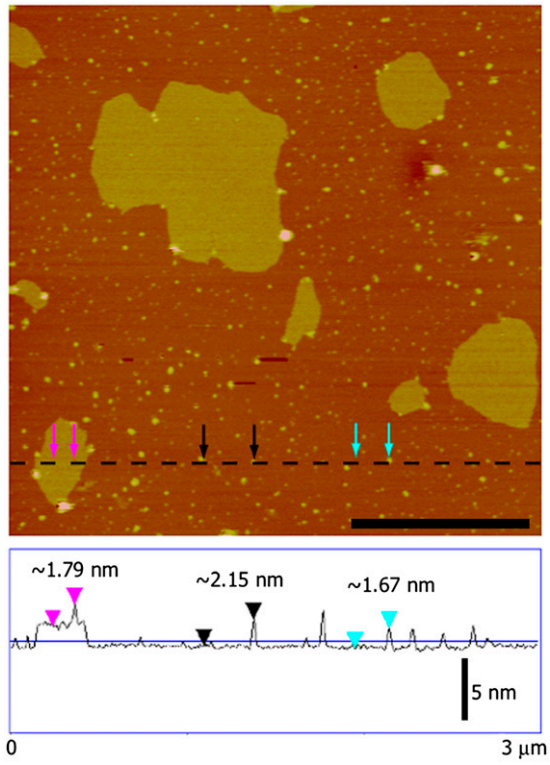

FIGURE 7 In situ TMAFM topography (height) imaging of the interactions between Tet C and 1 mol % G_{T1b}/DPOPC/DPPC lipid bilayers. After ~12 h incubation, Tet C was found to be preferentially associated with the fluid phase DPOPC regions of the bilayer. The morphology of the bilayer, however, remained relatively unchanged and no defects were observed to have formed. Cross section analysis found the Tet C molecules to extend ~2 nm above the surface of both the DPOPC and the DPPC domains. The AFM image is height-encoded by color where lighter colors correspond to taller features. Height scale, 15 nm; scale bar, 1 μm.

toxin was determined by lipid headgroup charge and conformation, as well as acyl chain length, with all of these factors being best fulfilled by the ganglioside G_{T1b}. These observations suggest that electrostatic interactions play a large role in the binding of TeNT to the G_{T1b} receptor. As the Tet C fragment is the membrane-binding domain, it is likely that its interactions with G_{T1b} would be sensitive to changes in pH. This result is in contrast to work by others who have examined the formation of pores in lipid membranes by the full-length tetanus toxin at low pH (57–60).

The results of these studies clearly indicate that at physiological pH (7.4) the tetanus toxin C-fragment binds to the fluid phase regions of G_{T1b}-containing membranes and after prolonged exposure, appears to organize into structures or assemblies that generate fairly uniform and relatively large cavity depressions within these regions. The gel phase domains, however, were relatively resistant to Tet C binding and activity. Our preliminary studies also suggest a threshold G_{T1b} concentration is necessary to initiate Tet C association and cavity formation, although at this time we cannot confirm whether the distribution of G_{T1b} is uniform throughout the model membranes. Studies by Winter et al. of the full-length tetanus neurotoxin (TeNT) also found that a critical concentration of G_{T1b} was necessary for pore formation in phosphatidylcholine lipid vesicles (61). Calorimetric measurements indicated that each TeNT molecule required 20 bound G_{T1b} molecules to adopt the correct conformation for stable pore formation.

Cross section analysis performed on the larger cavities formed in the DPOPC-rich areas revealed that they extend ~1.5 nm into the bilayer and do not span the entire SPB to expose the underlying mica surface (Fig. 6 *c*). Although the cavities themselves do not have the characteristics of transmembrane pores, they may instead be precursors toward the formation of the smaller membrane pores (estimated at ~2 nm diameter for tetanus neurotoxin) (15) or perhaps the initial stages of endosome formation. Neuronal endosomes are known to form within the size range of these observed cavities (62). The presence of a fluorescence signal in the areas of the defects in the correlated TIRFM images indicates that Tet C was present within the cavities, which likely contributed to their stability over extended periods of AFM imaging (greater than hours) (Fig. 6 *b*). Choi and Dimitriadis performed in situ AFM studies of the binding of cytochrome *c* to anionic lipid bilayers (61). At higher concentrations, cytochrome *c* was found to insert into the fluid phase bilayers and over time, formed circular defects in the bilayers. The authors believed that the defects were nanodomains of pure protein. Studies by others have suggested that the Tet C fragment itself does not form pores in lipid bilayers (18,57–59,63). This model is in reasonable agreement with our studies where Tet C appears to affect only the upper leaflet of the bilayer. In the context of this study, we cannot discount the possibility that this effect is specific to the use of a supported planar lipid bilayer model of a membrane.

We note that the larger size of the cavities observed in our combined TMAFM/TIRFM studies may be attributed to the higher concentration of FITC-labeled Tet C used. Sharpe and London found that the size of the pores formed by the A_1B_1-diphtheria toxin in lipid vesicles increased with increasing toxin concentration (64). The authors believed that the change in pore size was due to the oligomerization of the diphtheria molecules, with the number of toxin subunits determining the size of the pore formed in the membrane. In our AFM studies, we did not observe the formation of any supramolecular assemblies of Tet C on the surface of the lipid bilayer before the appearance of the cavity structures.

The insertion of Tet C into the fluid phase regions of the lipid bilayer and concomitant cavity formation may explain the observed increase in the thickness of these areas after the ~12-h incubation period. This process would likely cause tighter packing of the DPOPC molecules, and hence a decrease in the tilt angle of their acyl chains and subsequent increase in the height of these regions (36–38). As cell membranes are dynamic in nature, this change in the morphology of the bilayer may reflect an actual physiological cellular response. Cantor proposed a mechanism whereby changes in the lateral pressure of a cell membrane can affect the behavior of membrane proteins, thereby influencing cell surface recognition and initiating intracellular signaling events (65,66).

In addition to the circular cavities found throughout the fluid phase of the 10 mol % G_{T1b}/DPOPC/DPPC lipid bilayers, prominent defects were found at the border between the gel phase DPPC domains and the fluid phase DPOPC lipid matrix (Figs. 4, *b* and *c*, and 5). These defects exist between the intact DPPC and granular, cavity-filled DPOPC domains, and were found on both the leading and trailing edges, as defined by the scanning AFM tip, of various domains, suggesting that these structures are not imaging artifacts. Indeed, Barlic et al. found that the pore-forming equinatoxin-II preferentially binds at the boundaries between the ordered and disordered phases in biphasic membranes (67). They proposed that lipid packing defects and differences in the membrane thickness occurring at these interfaces may facilitate favorable interactions with the toxin. As Tet C inserts into the lipid bilayer, we are unable to detect by AFM, any accumulation of Tet C at the interface between the DPOPC and DPPC lipid phases. Ideally, we would be able to characterize, using TIRFM, any accumulation of Tet C at these interfaces as an increase in the intensity of the fluorescence emission in these regions. Unlike AFM, however, TIRFM is a diffraction-limited technique. With such a large amount of fluorescently labeled Tet C present throughout the DPOPC fluid phase of the bilayer contributing to the overall fluorescence emission, it was difficult to resolve whether the intensity within the DPOPC regions differs from that at the DPOPC-DPPC interfaces. Nevertheless, our observations of the membrane-disruptive activity of the C-fragment of the A_1B_1-tetanus toxin may have physiological relevance as it suggests that Tet C may actually be involved or aid in the

formation of a ''true'' membrane pore by the full-length TeNT.

CONCLUSIONS

This study provides the first direct nanoscale observation of the binding and interactions between the tetanus toxin C-fragment (Tet C) and supported lipid bilayers containing the ganglioside receptor G_{T1b}. As opposed to a number of ion channel studies with tetanus toxin that have employed suspended lipid membranes lacking a recognized toxin receptor, we found that G_{T1b} was essential for toxin binding and activity on the membrane surface (58,59). Furthermore, we observed preferential association of Tet C with the G_{T1b}-containing fluid phase regions in gel-fluid biphasic membranes. Over time, these interactions facilitated a dramatic change in the morphology of the supported lipid bilayer that resulted in the formation of 40–80 nm cavities with a concomitant increase in the thickness of the fluid phase regions of the bilayer upon insertion of bound Tet C. We also found that the membrane activity of Tet C was dependent upon both the ganglioside concentration in the membrane and solution pH.

Although TMAFM studies were unable to resolve Tet C on the surface of the lipid bilayer after the structural change in the fluid phase regions had occurred, combined TMAFM/TIRFM studies were able to confirm that Tet C is indeed present in the bilayer. This demonstrates the power of this coupled approach for performing functional imaging of lipid membranes and specifically ligand/protein-membrane interactions. The results of these studies now provide us with the framework necessary to perform in situ AFM studies of the membrane interactions and subsequent pore formation by the full-length tetanus toxin.

We gratefully acknowledge the generous support of the Canadian Institutes of Health Research (MT-14769), the Natural Sciences and Engineering Research Council of Canada (194435-99), the Canada Foundation for Innovation, the Ontario Research and Development Challenge Fund, the Ontario Innovation Trust, and the U.S. Department of Energy Office of Basic Energy Sciences. C.M.Y. is a Canada Research Chair in Molecular Imaging. A.L.S. thanks the Natural Sciences and Engineering Research Council of Canada for fellowship support. Sandia is a multiprogram laboratory operated by Sandia Corporation, a Lockheed Martin Company, for the U.S. Department of Energy's National Nuclear Security Administration under contract DE-AC04-94AL85000.

REFERENCES

1. Henderson, D. A. 1999. The looming threat of bioterrorism. *Science*. 283:1279–1282.
2. Bellamy, R. J., and A. R. Freedman. 2001. Bioterrorism. *Q. J. Med.* 94:227–234.
3. Montecucco, C. 1986. How do tetanus and botulinum toxins bind to neuronal membranes? *Trends Biochem. Sci.* 11:314–317.
4. Louch, H. A., E. S. Buczko, M. A. Woody, R. M. Venable, and W. F. Vann. 2002. Identification of a binding site for ganglioside on the receptor binding domain of tetanus toxin. *Biochemistry*. 41:13644–13652.
5. Pellizzari, R., O. Rossetto, G. Schiavo, and C. Montecucco. 1999. Tetanus and botulinum neurotoxins: mechanism of action and therapeutic uses. *Philos. Trans. R. Soc. Lond. B Biol. Sci.* 354:259–268.
6. Halpern, J. L., and E. A. Neale. 1995. Neurospecific binding, internalization, and retrograde axonal transport. *Curr. Top. Microbiol. Immunol.* 195:221–241.
7. Lalli, G., S. Bohnert, K. Deinhardt, C. Verastegui, and G. Schiavo. 2003. The journey of tetanus and botulinum neurotoxins in neurons. *Trends Microbiol.* 11:431–437.
8. Turton, K., J. A. Chaddock, and K. R. Acharya. 2002. Botulinum and tetanus neurotoxins: structure, function and therapeutic utility. *Trends Biochem. Sci.* 27:552–558.
9. Schiavo, G., F. Benfenati, B. Poulain, O. Rossetto, P. Polverino de Laureto, B. R. DasGupta, and C. Montecucco, 1992. Tetanus and botulinum-B neurotoxins block neurotransmitter release by proteolytic cleavage of synaptobrevin. *Nature*. 359:832–835.
10. Puhar, A., E. A. Johnson, O. Rossetto, and C. Montecucco. 2004. Comparison of the pH-induced conformational change of different clostridial neurotoxins. *Biochem. Biophys. Res. Commun.* 319:66–71.
11. Montecucco, C., G. Schiavo, J. Brunner, E. Duflot, Boquet, and M. Roa, 1986. Tetanus toxin is labeled with photoactivatable phospholipids at low pH. *Biochemistry*. 25:919–924.
12. Donovan, J. J., M. I. Simon, R. K. Draper, and M. Montal. 1981. Diphtheria toxin forms transmembrane channels in planar lipid bilayers. *Proc. Natl. Acad. Sci. USA*. 78:172–176.
13. Kagan, B. L., A. Finkelstein, and M. Colombini. 1981. Diphtheria toxin fragment forms large pores in phospholipid bilayer membranes. *Proc. Natl. Acad. Sci. USA*. 78:4950–4954.
14. Deleers, M., N. Beugnier, P. Falmagne, V. Cabiaux, and J. M. Ruysschaert. 1983. Localization in diphtheria toxin fragment B of a region that induces pore formation in planar lipid bilayers at low pH. *FEBS Lett.* 160:82–86.
15. Hoch, D. H., M. Romero-Mira, B. E. Ehrlich, A. Finkelstein, B. R. DasGupta, and L. L. Simpson. 1985.Channels formed by botulinum, tetanus, and diphtheria toxins in planar lipid bilayers: relevance to translocation of proteins across membranes. *Proc. Natl. Acad. Sci. USA*. 82: 1692–1696.
16. Donovan, J. J., and J. L. Middlebrook. 1986. Ion-conducting channels produced by botulinum toxin in planar lipid membranes. *Biochemistry*. 25:2872–2876.
17. Blaustein, R. O., T. M. Koehler, R. J. Collier, and A. Finkelstein. 1989. Anthrax toxin: channel-forming activity of protective antigen in planar phospholipid bilayers. *Proc. Natl. Acad. Sci. USA*. 86:2209–2213.
18. Beise, J., J. Hahnen, B. Andersen-Beckh, and F. Dreyer. 1994. Pore formation by tetanus toxin, its chain and fragments in neuronal membranes and evaluation of the underlying motifs in the structure of the toxin molecule. *Naunyn Schmiedebergs Arch. Pharmacol.* 349:66–73.
19. Cabiaux, V., C. Wolff, and J. M. Ruysschaert. 1997. Interaction with a lipid membrane: a key step in bacterial toxins virulence. *Int. J. Biol. Macromol.* 21:285–298.
20. Qiu, X.Q., K.S. Jakes, P.K. Kienker, A. Finkelstein, A., and S. L. Slatin, 1996. Major transmembrane movement associated with colicin Ia channel gating. *J. Gen. Physiol.* 107:313–328.
21. Santos, N. C., E. Ter-Ovanesyan, J. A. Zasadzinski, M. Prieto, and M. A. Castanho. 1998. Filipin-induced lesions in planar phospholipid bilayers imaged by atomic force microscopy. *Biophys. J.* 75:1869–1873.
22. Milhaud, J., V. Ponsinet, M. Takashi, and B. Michels. 2002. Interactions of the drug amphotericin B with phospholipid membranes containing or not ergosterol: new insight into the role of ergosterol. *Biochim. Biophys. Acta.* 1558:95–108.
23. Steinem, C., H.-J. Galla, and A. Janshoff. 2000. Interaction of melittin with solid supported membranes. *Phys. Chem. Chem. Phys.* 2:4580–4585.
24. Yip, C. M., and J. McLaurin. 2001. Amyloid-beta peptide assembly: a critical step in fibrillogenesis and membrane disruption. *Biophys. J.* 80:1359–1371.

25. Jo, E., J. McLaurin, C. M. Yip, P. St George-Hyslop, and P. E. Fraser. 2000. α-Synuclein membrane interactions and lipid specificity. *J. Biol. Chem.* 275:34328–34334.

26. Epand, R. F., C. M. Yip, V. Chernomordik, L. D. Le, Y. K. Duc, Y. K. Shin, and R. M. Epand. 2001. Self-assembly of influenza hemagglutinin: studies of ectodomain aggregation by in situ atomic force microscopy. *Biochim. Biophys. Acta.* 1513:167–175.

27. Epand, R. F., J. C. Martinou, S. Montessuit, R. M. Epand, and C. M. Yip. 2002. Direct evidence for membrane pore formation by the apoptotic protein Bax. *Biochem. Biophys. Res. Commun.* 298:744–749.

28. Epand, R. M., S. Maekawa, C. M. Yip, and R. F. Epand. 2001. Protein-induced formation of cholesterol-rich domains. *Biochemistry.* 40: 10514–10521.

29. Bayerl, T. M., and M. Bloom. 1990. Physical properties of single phospholipid bilayers adsorbed to micro glass beads: a new vesicular model system studied by 2H-nuclear magnetic resonance. *Biophys. J.* 58:357–362.

30. Johnson, S. J., T. M. Bayerl, D. C. McDermott, G. W. Adam, A. R. Rennie, R. K. Thomas, and E. Sackmann. 1991. Structure of an adsorbed dimyristoylphosphatidylcholine bilayer measured with specular reflection of neutrons. *Biophys. J.* 59:289–294.

31. Salafsky, J., J. T. Groves, and S. G. Boxer. 1996. Architecture and function of membrane proteins in planar supported bilayers: a study with photosynthetic reaction centers. *Biochemistry.* 35:14773–14781.

32. Slade, A., J. Luh, S. Ho, and C. M. Yip. 2002. Single molecule imaging of supported planar lipid bilayer-reconstituted human insulin receptors by in situ scanning probe microscopy. *J. Struct. Biol.* 137: 283–291.

33. Shaw, J. E., A. Slade, and C. M. Yip. 2003. Simultaneous in situ total internal reflectance fluorescence/atomic force microscopy studies of DPPC/dPOPC microdomains in supported planar lipid bilayers. *J. Am. Chem. Soc.* 125:11838–11839.

34. Fotinou, C., P. Emsley, I. Black, H. Ando, H. Ishida, M. Kison, K. A. Sinha, N. F. Fairweather, and N. W. Isaacs. 2001. The crystal structure of tetanus toxin Hc fragment complexed with a synthetic GT1b analogue suggests cross-linking between ganglioside receptors and the toxin. *J. Biol. Chem.* 276:32274–32281.

35. Maeda, H. 1997. An atomic force microscopy study for the assembly structures of tobacco mosaic virus and their size evaluation. *Langmuir.* 13:4150–4161.

36. Mou, J., J. Yang, C. Huang, and Z. Shao. 1994. Alcohol induces interdigitated domains in unilamellar phosphatidylcholine bilayers. *Biochemistry.* 33:9981–9985.

37. Masai, J., T. Shibataseki, K. Sasaki, H. Murayama, and K. Sano. 1996. Scanning force microscopy characterization of thin lipid films on a substrate. *Thin Solid Films.* 273:289–296.

38. Hollars, C. W., and R. C. Dunn. 1998. Submicron structure in L-α-dipalmitoylphosphatidylcholine monolayers and bilayers probed with confocal, atomic force, and near-field microscopy. *Biophys. J.* 75:342–353.

39. McKiernan, A. E., T. V. Ratto, and M. L. Longo. 2000. Domain growth, shapes, and topology in cationic lipid bilayers on mica by fluorescence and atomic force microscopy. *Biophys. J.* 79:2605–2615.

40. Giocondi, M.-C., V. Vie, E. Lesniewska, P.-E. Milhiet, M. Zinke-Allmang, and C. Le Grimellec. 2001. Phase topology and growth of single domains in lipid bilayers. *Langmuir.* 17:1653–1659.

41. Brown, D. A., and E. London. 2000. Structure and function of sphingolipid- and cholesterol-rich membrane rafts. *J. Biol. Chem.* 275:17221–17224.

42. Simons, K., and D. Toomre. 2000. Lipid rafts and signal transduction. *Nat. Rev. Mol. Cell Biol.* 1:31–39.

43. Simons, K., and E. Ikonen. 1997. Functional rafts in cell membranes. *Nature.* 387:569–572.

44. Rietveld, A., and K. Simons. 1998. The differential miscibility of lipids as the basis for the formation of functional membrane rafts. *Biochim. Biophys. Acta.* 1376:467–479.

45. Mou, J., J. Yang, and Z. Shao. 1995. Atomic force microscopy of cholera toxin B-oligomers bound to bilayers of biologically relevant lipids. *J. Mol. Biol.* 248:507–512.

46. Yuan, C., and L. J. Johnston. 2000. Distribution of ganglioside GM1 in L-α-dipalmitoylphosphatidylcholine/cholesterol monolayers: a model for lipid rafts. *Biophys. J.* 79:2768–2781.

47. Yuan, C., and L. J. Johnston. 2001. Atomic force microscopy studies of ganglioside GM1 domains in phosphatidylcholine and phosphatidylcholine/cholesterol bilayers. *Biophys. J.* 81:1059–1069.

48. Mehlhorn, I. E., G. Parrag, K. R. Barber, and C. W. Grant. 1986. Visualization of domains in rigid ganglioside/phosphatidylcholine bilayers: Ca^{2+} effects. *Biochim. Biophys. Acta.* 863:139–155.

49. Last, J. A., T. A. Waggoner, and D. Y. Sasaki. 2001. Lipid membrane reorganization induced by chemical recognition. *Biophys. J.* 81:2737–2742.

50. Sasaki, D. Y., T. A. Waggoner, J. A. Last, J and T. M. Alam. 2002. Crown ether functionalized membranes: lead ion recognition and molecular reorganization. *Langmuir.* 18:3714–3721.

51. Cruz, A., L. Vazquez, M. Velez, and J. Perez-Gil. 2005. Influence of a fluorescent probe on the nanostructure of phospholipid membranes: dipalmitoylphosphatidylcholine interfacial monolayers. *Langmuir.* 21: 5349–5355.

52. Saez-Cirion, A., S. Nir, M. Lorizate, A. Agirre, A. Cruz, J. Perez-Gil, and J. L. Nieva. 2002. Sphingomyelin and cholesterol promote HIV-1 gp41 pretransmembrane sequence surface aggregation and membrane restructuring. *J. Biol. Chem.* 277:21776–21785.

53. Bernardino de la Serna, J., J. Perez-Gil, A. C. Simonsen, and L. A. Bagatolli. 2004.Cholesterol rules: direct observation of the coexistence of two fluid phases in native pulmonary surfactant membranes at physiological temperatures. *J. Biol. Chem.* 279:40715–40722.

54. Winter, A., W. P. Ulrich, F. Wetterich, U. Weller, and H. J. Galla. 1996. Gangliosides in phospholipid bilayer membranes: Interaction with tetanus toxin. *Chem. Phys. Lipids.* 81:21–34.

55. Boquet, P., and E. Duflot. 1982. Tetanus toxin fragment forms channels in lipid vesicles at low pH. *Proc. Natl. Acad. Sci. USA.* 79:7614–7618.

56. Gambale, F., and M. Montal. 1988. Characterization of the channel properties of tetanus toxin in planar lipid bilayers. *Biophys. J.* 53:771–783.

57. Menestrina, G., S. Forti, and F. Gambale. 1989. Interaction of tetanus toxin with lipid vesicles: effects of pH, surface charge, and transmembrane potential on the kinetics of channel formation. *Biophys. J.* 55: 393–405.

58. Calappi, E., M. Masserini, G. Schiavo, C. Montecucco, and G. Tettamanti. 1992. Lipid interaction of tetanus neurotoxin. A calorimetric and fluorescence spectroscopy study. *FEBS Lett.* 309:107–110.

59. Winter, A., W. P. Ulrich, F. Wetterich, U. Weller, and H. J. Galla. 1996. Gangliosides in phospholipid bilayer membranes: interaction with tetanus toxin. *Chem. Phys. Lipids.* 81:21–34.

60. Zhang, B., B. Ganetzky, H. J. Bellen, and V. N. Murthy. 1999. Tailoring uniform coats for synaptic vesicles during endocytosis. *Neuron.* 23:419–422.

61. Roa, M., and P. Boquet. 1985. Interaction of tetanus toxin with lipid vesicles at low pH: protection of specific polypeptides against proteolysis. *J. Biol. Chem.* 260:6827–6835.

62. Sharpe, J. C., and E. London. 1999. Diphtheria toxin forms pores of different sizes depending on its concentration in membranes: probable relationship to oligomerization. *J. Membr. Biol.* 171:209–221.

63. Cantor, R. S. 1997. Lateral pressures in cell membranes: a mechanism for modulation of protein function. *J. Phys. Chem. B.* 101:1723–1725.

64. Cantor, R. S. 1999. Lipid composition and the lateral pressure profile in bilayers. *Biophys. J.* 76:2625–2639.

65. Barlic, A., I, Gutierrez-Aguirre, J. M. Caaveiro, A. Cruz, M. B. Ruiz-Arguello, J. Perez-Gil, J., and J. M. Gonzalez-Manas, 2004. Lipid phase coexistence favors membrane insertion of equinatoxin-II, a pore-forming toxin from Actinia equina. *J. Biol. Chem.* 279:34209–34216.